Application of second-harmonic generation to retardation measurements

Stefano Cattaneo and Martti Kauranen

Optics Laboratory, Institute of Physics, Tampere University of Technology, P.O. Box 692, FIN-33101 Tampere, Finland

Received June 14, 2002; revised manuscript received October 22, 2002

The efficiency of second-harmonic generation from thin films by use of two input beams at the fundamental frequency depends sensitively on the polarization states of the fundamental beams. This dependence allows precise measurement of the retardation induced by optical elements. We present a theoretical analysis of the technique and discuss its advantages and limitations with regard to retardation measurements. We demonstrate our technique by measuring the retardation of a commercial half-wave plate to a precision and repeatability of better than $\lambda/10^4$. The technique is remarkably insensitive to misalignments of the optical components and of the fundamental beams for the retardation range investigated ($\delta = 180 \pm 10°$). The extension of the technique to measure low values of retardation ($\delta \sim 0°$) is straightforward.

OCIS codes: 190.0190, 120.5410, 260.1440.

1. INTRODUCTION

Polarization is an essential parameter in the characterization of vectorial waves and is therefore a fundamental property of light.[1,2] Many processes that involve light depend on polarization. The polarization of light that travels through a medium is sensitive to its optical properties.[2] For this reason, the study of polarization is a powerful tool in spectroscopy and has a plenitude of applications in, e.g., chemistry, biology, astronomy, and remote sensing.[3–6] In fiber optics, polarization mode dispersion is a key factor that limits transmission speed.[7]

An arbitrary (elliptical) polarization state is completely specified by two parameters: the azimuth (direction of the major axis of the polarization ellipse) and the ellipticity (ratio between the minor and the major axes of the ellipse, which usually includes the handedness of the ellipse). Alternatively, the polarization state can be defined by the relative amplitudes of two arbitrary orthogonal polarization components and the phase difference (retardation) between them.[8]

It is difficult to measure polarization precisely. The orientation of the polarization ellipse can be determined to a precision of 10^{-6} rad by use of existing ellipsometric techniques.[9] The retardation induced by active components has been measured to a precision of the order of $\lambda/10^8$ by use of, e.g., an intracavity polarimeter[10] or optical heterodyne techniques.[11] With passive components, a similar precision has been reached only for specific cases, e.g., for supermirrors with ultralow birefringence.[12] However, accurate measurement of the ellipticity of an arbitrary beam or of the retardation induced by common birefringent elements remains a challenging task.

Characterization of wave plates illustrates the problems encountered in retardation measurements. Wave plates are commonly used to control or analyze polarization. They operate by resolving light into two orthogonal polarization components and by producing a phase shift between them. The phase shift determines the polarization of the resulting light wave. In optical industry, retardation of wave plates can nowadays be measured to a precision of $\lambda/1000$ by ellipsometric techniques.[13]

Considerable effort has been put into increasing the accuracy of retardation measurements by improving traditional techniques or by developing alternative methods.[14–19] Some techniques reach a precision of $\lambda/7000$ but require complicated experimental arrangements or data analysis.[14–17] Recently, a technique based on polarization modulation[18,19] quoted a sensitivity of the order of $\lambda/10^5$. However, a relative uncertainty of 1% limits the technique to low values of retardation.[19] Existing techniques often rely on careful alignment of several polarization components. Their absolute precision is then considerably lower than the quoted sensitivity.

Second-order nonlinear optical processes are sensitive probes of material symmetry. For example, thin films of low symmetry can have characteristic signatures in their nonlinear response.[20–22] Such sensitivity arises from the tensor nature of the nonlinear response, which also results in a sensitive dependence on polarization. Second-order crystals, for example, have already been used as polarizers and analyzers.[23]

The polarization sensitivity of nonlinear processes suggests that nonlinear techniques could also be used to determine an arbitrary polarization state of an optical beam. We recently pursued this idea by developing a nonlinear technique based on second-harmonic generation to measure optical retardation.[24] We used two beams at the fundamental frequency to generate second-harmonic light from a polymer film. The sensitive polarization dependence of the process allows measurement of the retardation of one fundamental beam in a precise way. The technique relies on symmetry properties of the nonlinear interactions and does not require sophisticated experimental arrangement or data analysis to achieve high

precision. In our initial demonstration of the technique, we already achieved a precision of $\lambda/10^4$.

Here we present a theoretical analysis of our technique and discuss its advantages and limitations with regard to retardation measurements. Special attention is given to the optimization of the experimental geometry and to practical issues that concern data analysis. We also describe the retardation measurements performed to demonstrate our technique and address various sources of possible errors in the technique.

2. THEORETICAL FRAMEWORK

The geometry of the technique is illustrated in Fig. 1. Two beams ($\mathbf{E}_1$ and $\mathbf{E}_2$) at fundamental frequency ω are applied to the same spot of a thin nonlinear film. The beams are in the same plane of incidence with respect to the sample, with angles of incidence θ_1 and θ_2 and wave vectors $\mathbf{k}_1$ and $\mathbf{k}_2$. The coordinates x and y are in the plane of the film, and z is along the film normal. More specifically, x and y, respectively, are parallel and perpendicular to the plane of incidence. The propagation directions of the beams are then given by unit vectors $\hat{k}_i = \sin\theta_i\hat{x} - \cos\theta_i\hat{z}$.

Our technique is based on the general symmetry properties of the nonlinear interaction rather than on its details. Therefore we simplify our model by assuming unity linear refractive indices for the film and the media surrounding it. This assumption allows us to maintain mathematical simplicity in the theoretical description of the technique, while fully accounting for its salient features. The assumption is waived in the actual retardation measurements. In this model, the Cartesian components of the nonlinear polarization $\mathbf{P}$ at frequency 2ω are

$$P_i = \chi^{(2)}_{ijk} E_j E_k , \tag{1}$$

where $\mathbf{E} = \mathbf{E}_1 + \mathbf{E}_2$ is the total incoming field and $\chi^{(2)}_{ijk}$ is the second-harmonic susceptibility tensor. The subscripts *ijk* refer to the *x,y,z* coordinates and summation over repeated indices is implied. The amplitude of the second-harmonic field emitted in direction $\mathbf{n}$ is proportional to[25]

$$\mathbf{E}_3 \sim [\mathbf{n} \times \mathbf{P}] \times \mathbf{n}. \tag{2}$$

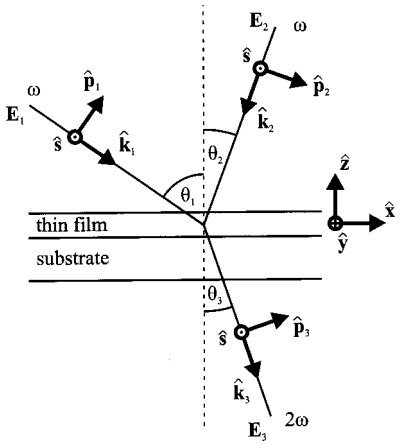

Fig. 1. Geometry of nonlinear retardation measurements. Two beams (target and probe) at the fundamental frequency ω are applied to the same spot on a poled thin film and coherent second-harmonic light in the sum direction is detected. All beams are on the same plane of incidence. Note that angles θ_1 and θ_2 are drawn as positive and negative, respectively.

The planar extension of the nonlinear material provides a phase-matching condition in the x and y directions. Coherent second-harmonic beams are then observed along $2\mathbf{k}_1$ and $2\mathbf{k}_2$ as results of processes driven by each fundamental beam separately. In addition, the two beams jointly lead to a second-harmonic beam in a third direction $\mathbf{k}_3$ in the same plane of incidence. Since the component of the wave vector in the plane of the film is conserved, the propagation angle θ_3 of this beam is given by[26] $\sin\theta_3 = (\sin\theta_1 + \sin\theta_2)/2$.

The fields $\mathbf{E}_i$ ($i = 1, 2, 3$) are most naturally expressed as a sum of p (parallel to the plane of incidence) and s (normal to the plane of incidence) components, $\mathbf{E}_i = E_{is}\hat{s} + E_{ip}\hat{p}_i$. The s direction is the same for all beams ($\hat{s} = -\hat{y}$), whereas the p direction depends on the propagation direction $\hat{p}_i = \hat{s} \times \hat{k}_i$. The components of $\mathbf{E}_i$ in the two reference systems are related by

$$E_{ix} = E_{ip}\cos\theta_i , \quad E_{iy} = -E_{is} , \quad E_{iz} = E_{ip}\sin\theta_i . \tag{3}$$

Equation (2) yields the components of the second-harmonic field emitted in direction $\mathbf{n} = \hat{k}_3$:

$$E_{3x} = (P_x\cos\theta_3 + P_z\sin\theta_3)\cos\theta_3 , \tag{4}$$

$$E_{3y} = P_y , \tag{5}$$

$$E_{3z} = (P_x\cos\theta_3 + P_z\sin\theta_3)\sin\theta_3 . \tag{6}$$

Throughout this paper we consider a thin film of $C_{\infty v}$ symmetry (such as an achiral poled polymer film). Such a sample is isotropic in the plane of the film but has a second-order nonlinear response that is due to broken symmetry along the film normal. The nonvanishing components *ijk* of tensor $\chi^{(2)}_{ijk}$ are then zzz, $zxx = zyy$, $xxz = xzx = yyz = yzy$. Using Eqs. (3)–(6), we found the following general forms for the components of the second-harmonic field[27]

$$E_{3p} = f_p E_{1p} E_{2p} + g_p E_{1s} E_{2s} . \tag{7}$$

$$E_{3s} = f_s E_{1p} E_{2s} + g_s E_{1s} E_{2p} . \tag{8}$$

The expansion coefficients f_i and g_i are linear combinations of the components of $\chi^{(2)}_{ijk}$ and depend on angles θ_i:

$$\begin{aligned} f_p = {} & 2\chi^{(2)}_{xxz}\sin\theta_1\cos\theta_2\cos\theta_3 \\ & + 2\chi^{(2)}_{xxz}\cos\theta_1\sin\theta_2\cos\theta_3 \\ & + 2\chi^{(2)}_{zxx}\cos\theta_1\cos\theta_2\sin\theta_3 \\ & + 2\chi^{(2)}_{zzz}\sin\theta_1\sin\theta_2\sin\theta_3 , \end{aligned} \tag{9}$$

$$g_p = 2\chi^{(2)}_{zxx}\sin\theta_3, \tag{10}$$

$$f_s = 2\chi^{(2)}_{xxz}\sin\theta_1 , \tag{11}$$

$$g_s = 2\chi^{(2)}_{xxz}\sin\theta_2 , \tag{12}$$

We obtained Eqs. (9)–(12) by assuming unity refractive indices for all the materials. A complete treatment including the indices of refraction of the various materials

and other complicating factors is straightforward.[28] In the analysis of experimental results we used only the general Eqs. (7) and (8), which remain valid also in the complete treatment, since they are a pure consequence of the symmetry of the sample.

3. POLARIZATION EFFECTS

As already pointed out, second-harmonic generation depends sensitively on polarization. Therefore, a careful analysis of the second-harmonic signal yields information about the polarizations of the fundamental beams. In our technique, the polarization of one beam (target beam, wave vector $\mathbf{k}_1$) is determined by measurement of the dependence of the second-harmonic signal on the polarization of the other beam (probe beam, wave vector $\mathbf{k}_2$).

Previous research with poled films showed that a circularly polarized target beam results in a different response of second-harmonic generation to left- and right-hand circularly polarized probe beams.[27] The difference effect can be quantified by the normalized circular-difference response in the second-harmonic signal intensity

$$\frac{\Delta I}{I} = \frac{I_{\text{left}} - I_{\text{right}}}{(I_{\text{left}} + I_{\text{right}})/2}, \tag{13}$$

where the subscripts refer to circular probe polarizations. A circular-difference response occurs also with elliptical target polarization, which can be described as the sum of linear and circular components. Moreover, the difference response depends on the ellipticity of the target beam, which determines the relative amplitudes of the circular and linear polarization components.

To understand the origin of the circular-difference effect, we calculate the response when the probe beam is circularly polarized, i.e., $E_{2s} = \pm iE_{2p}$, where the + and − signs correspond to left- and right-hand circular polarizations, respectively. From Eqs. (7) and (8) we then determine that the intensities of the p and s components of the second-harmonic field are proportional to

$$|E_{3p}|^2 = [|f_p|^2|E_{1p}|^2 + |g_p|^2|E_{1s}|^2 \pm i(f_p^* g_p E_{1s} E_{1p}^* - f_p g_p^* E_{1s}^* E_{1p})]|E_{2p}|^2, \tag{14}$$

$$|E_{3s}|^2 = [|f_s|^2|E_{1p}|^2 + |g_s|^2|E_{1s}|^2 \pm i(f_s g_s^* E_{1s}^* E_{1p} - f_s^* g_s E_{1s} E_{1p}^*)]|E_{2p}|^2, \tag{15}$$

Equations (14) and (15) show that there are two possible sources of a circular-difference effect: a phase difference between a pair of expansion coefficients f_i and g_i or a phase difference between the polarization components of the target beam.

For our measurement technique, a phase difference between f_i and g_i constitutes a limitation. In general, the components of $\chi_{ijk}^{(2)}$ are complex numbers. Equations (9)–(12) show that phase differences between susceptibility components will result in phase differences between expansion coefficients. However, for poled films that contain chromophores with a single charge-transfer axis, the nonvanishing components of $\chi_{ijk}^{(2)}$ are $zxx = zyy = xxz = xzx = yyz = yzy = zzz/r$, where r is the (real) poling ratio,[29] and no phase differences occur between them. Nevertheless, the most general expressions for f_i and g_i depend on linear (complex) refractive indices and propagation effects. Hence, the absence of phase differences between the coefficients f_i and g_i must be verified experimentally for the sample used.

When phase differences between expansion coefficients are excluded, the circular difference is determined by the imaginary part of $E_{1s}E_{1p}^*$. The only possible source for a circular-difference response is then a phase difference between the polarization components of the target beam, i.e., no circular-difference effect occurs for linear target polarization. An arbitrary phase difference between the target polarization components leads to a circular-difference response that arises directly from interference between the real and the imaginary parts of the target polarization vector. However, to access these interference effects, a phase difference between the components of the probe polarization vector must be introduced, for example, by use of circular probe polarizations, as was assumed in the derivation of Eqs. (14) and (15).

Let us consider a general elliptical target polarization (Fig. 2). With $2a$ and $2b$ as the lengths of the principal axes of the ellipse, the field components along the principal directions ξ and η are

$$E_{1\xi}(t) = a\exp(-i\omega t), \qquad E_{1\eta}(t) = \mp ib\exp(-i\omega t). \tag{16}$$

Here, the upper sign represents an ellipse of positive handedness (right-hand ellipse). Introducing the ellipticity $e = \pm b/a (-1 \leqslant e \leqslant 1)$, Eqs. (16) yield $E_{1\eta} = -ieE_{1\xi}$. The ellipticity e incorporates the handedness of the ellipse: it is positive for right-hand and negative for left-hand polarization.

When ψ is the azimuth of the polarization ellipse (angle between the major axis and the p direction, $0 < \psi \leqslant \pi$), the p and s components are

$$E_{1p} = E_{1\xi}\cos\psi - E_{1\eta}\sin\psi = (\cos\psi + ie\sin\psi)E_{1\xi}, \tag{17}$$

$$E_{1s} = E_{1\xi}\sin\psi + E_{1\eta}\cos\psi = (\sin\psi - ie\cos\psi)E_{1\xi}. \tag{18}$$

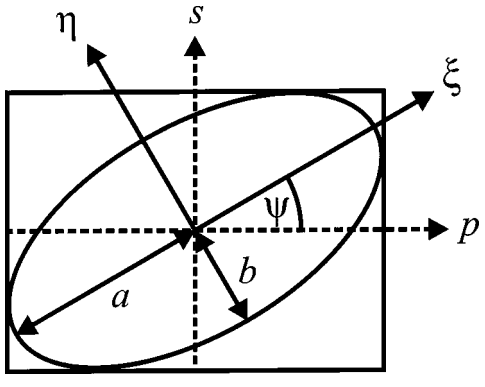

Fig. 2. Elliptically polarized target beam. The principal axes of the polarization ellipse are oriented along ξ and η. Azimuth ψ is the angle between the major axis and the p direction ($0 < \psi \leqslant \pi$). The lengths of major and minor axes of the ellipse are $2a$ and $2b$, respectively.

As discussed above, once phase differences between coefficients f_i and g_i are excluded, the circular-difference response is governed by the imaginary part of $E_{1s}E_{1p}^*$, which now is

$$\mathrm{Im}(E_{1s}E_{1p}^*) = -e|E_\xi|^2(\cos^2\psi + \sin^2\psi) = -ea^2. \tag{19}$$

As a consequence, the difference $I_{\mathrm{left}} - I_{\mathrm{right}}$ in the second-harmonic signal depends only on the ellipticity but not on the azimuth of the target polarization ellipse. However, the normalized circular-difference response [Eq. (13)] also depends on the azimuth.

4. MEASUREMENT OF WAVE-PLATE RETARDATION

Next we consider the potential of the polarization dependence of the nonlinear response to determine the retardation of wave plates. The wave plate under investigation is placed in the target beam, just before the sample.

In general, the polarization vector $\mathbf{E}$ of a beam after it traverses a wave plate is related to the field $\mathbf{E}^0$ before the wave plate by

$$\begin{bmatrix} E_p \\ E_s \end{bmatrix} = T_{\mathrm{wp}} \begin{bmatrix} E_p^0 \\ E_s^0 \end{bmatrix}, \tag{20}$$

where T_{wp} is the Jones matrix for a wave plate of retardation δ (Ref. 30):

$$T_{\mathrm{wp}} = \begin{pmatrix} \cos\delta/2 - i\cos 2\phi \sin\delta/2 & -i\sin 2\phi \sin\delta/2 \\ -i\sin 2\phi \sin\delta/2 & \cos\delta/2 + i\cos 2\phi \sin\delta/2 \end{pmatrix}, \tag{21}$$

and ϕ is the angle between the fast axis of the wave plate and the p direction. Retardations $\delta = \pi$ and $\pi/2$ correspond to half- and quarter-wave plates, respectively.

We take the target beam before the wave plate to be polarized along the p direction and assume $\phi = +45°$. This choice is experimentally favorable and will be justified later. The components of the target beam after the wave plate are then

$$E_{1p} = \cos(\delta/2)E_{1p}^0, \qquad E_{1s} = -i\sin(\delta/2)E_{1p}^0, \tag{22}$$

where E_{1p}^0 is the field amplitude of the target beam before the wave plate. Equations (7) and (8) yield the intensities of the p and s components of the second-harmonic field for the two circular probe polarizations:

$$|E_{3p}|^2 = |f_p\cos(\delta/2) \pm g_p\sin(\delta/2)|^2|E_{2p}|^2|E_{1p}^0|^2, \tag{23}$$

$$|E_{3s}|^2 = |f_s\cos(\delta/2) \mp g_s\sin(\delta/2)|^2|E_{2p}|^2|E_{1p}^0|^2. \tag{24}$$

Intensity I of the second-harmonic signal is then

$$I = |E_{3p}|^2 + |E_{3s}|^2 = [(|f_p|^2 + |f_s|^2)\cos^2(\delta/2) + (|g_p|^2 + |g_s|^2)\sin^2(\delta/2) \pm (f_pg_p^* - f_sg_s^* + f_p^*g_p - f_s^*g_s) \times \cos(\delta/2)\sin(\delta/2)]|E_{2p}|^2|E_{1p}^0|^2. \tag{25}$$

Equation (25) yields the difference response of second-harmonic generation to left- and right-hand circularly polarized probe beams:

$$I_{\mathrm{left}} - I_{\mathrm{right}} = (f_pg_p^* - f_sg_s^* + f_p^*g_p - f_s^*g_s) \times |E_{2p}|^2|E_{1p}^0|^2\sin\delta. \tag{26}$$

Equation (26) shows that any retardation δ different from $m\pi$ (m is an integer) results in a circular-difference response unless the factor that includes the expansion coefficients f_i and g_i vanishes.

As an example, we consider the case of a nominal half-wave plate. A deviation of the actual wave-plate retardation from $\lambda/2$ (or π) introduces a small circular component in the target polarization and therefore results in a circular-difference response. Assuming a small retardation error $\sigma = \delta - \pi \ll \pi$, one can approximate Eqs. (23) and (24) as

$$|E_{3p}|^2 = |f_p\sigma/2 \mp g_p|^2|E_{2p}|^2|E_{1p}^0|^2, \tag{27}$$

$$|E_{3s}|^2 = |f_s\sigma/2 \pm g_s|^2|E_{2p}|^2|E_{1p}^0|^2. \tag{28}$$

For a given component, a high circular-difference response is thus obtained when g_i and $f_i\sigma/2$ are of the same order of magnitude. This is the first condition for the geometry to be used. With Eqs. (11) and (12), one can show that a high circular-difference response for the s component of the second-harmonic field is achieved when $|\theta_2| \ll |\theta_1|$, i.e., when the probe beam is near normal incidence. However, if $\theta_2 = 0$, g_s vanishes [Eq. (12)] and no circular-difference response is observed. The condition for the p component of the second-harmonic field is less easily interpreted because of the more complicated angular dependence of coefficient f_p [Eq. (9)].

5. OPTIMIZATION OF THE EXPERIMENTAL GEOMETRY

For a precise retardation measurement, the polarization of the target beam before the wave plate must be known accurately. The most natural choice is linear polarization because of the high quality of linear polarizers. The ellipticity induced by a wave plate of arbitrary retardation δ can then be specified by angle ε ($\tan\varepsilon = e$, $-\pi/4 \leqslant \varepsilon \leqslant \pi/4$) (Ref. 8):

$$\sin 2\varepsilon = \sin 2\phi \sin\delta, \tag{29}$$

where ϕ is the angle between the fast axis of the wave plate and the incoming linear polarization. The magnitude of ε and, consequently, of ellipticity e are maximum when $\phi = \pm 45°$.

It is convenient to optimize the normalized circular-difference response [Eq. (13)] to achieve a better contrast in the measured intensities. As explained above, this quantity also depends on the azimuth of the target polarization ellipse. For $C_{\infty v}$ sample symmetry, it can be shown that the normalized response is maximum when the major axis of the polarization ellipse after the wave plate is oriented along the s direction.

We used a computer simulation to optimize the experimental arrangement for measurement of the retardation of a nominal half-wave plate. Some results are shown in

Fig. 3. We assumed a retardation error $\varepsilon = \lambda/1000$ in the wave plate. The beam before the wave plate was polarized along the p direction and the fast axis of the wave plate was rotated by 45° resulting in elliptical target polarization with the major axis along the s direction. Unity refractive indices of all materials and the ideal poling ratio 3 for the film were assumed.[29] The normalized circular-difference response was calculated as a function of incident angles of the target (θ_1) and the probe (θ_2) beams. For unpolarized detection, a maximum 4.3% normalized circular-difference response was obtained for small incident angles of the probe beam.

We also investigated the response for polarized detection of the second-harmonic signal. Detecting the p component reduces the overall maximum of the normalized circular difference to approximately 3.8%. With s-polarized detection, the overall maximum increases by an order of magnitude for even smaller angles of incidence of the probe beam. However, this improvement is compromised by a simultaneous decrease in the intensity of the s component.

The optimum incident angles $\theta_1 = 24°$ and $\theta_2 = -4.5°$ for unpolarized detection result from a trade-off between high difference effects and high second-harmonic intensity. With these angles, the circular-difference response is still high (approximately 4%), but the signal intensity for circular probe polarizations is approximately 1 order of magnitude higher than the intensity obtained when the circular-difference response alone is maximized (Fig. 3). With optimum incident angles, the p component of the second-harmonic signal for circular probe polarizations is approximately 75% of the total second-harmonic intensity.

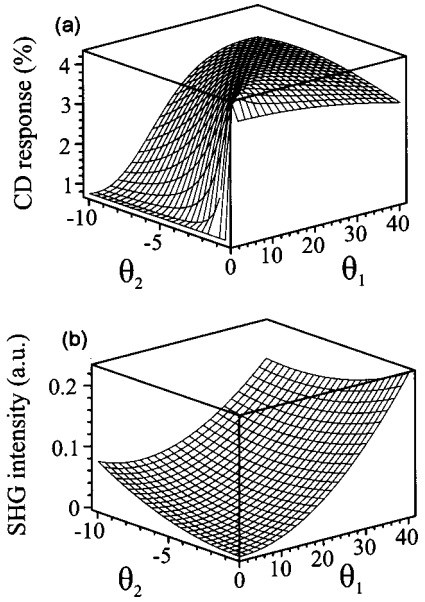

Fig. 3. Simulations for the case of unpolarized detection assuming a nominal half-wave plate with a retardation error of $\lambda/1000$. (a) Variation of the circular-difference (CD) response (%) on incident angles θ_1 and θ_2 (degrees) of target and probe beams, respectively. (b) Second-harmonic generation (SHG) intensity (a.u.) for right-hand circular probe polarization.

6. DATA ANALYSIS

So far we have focused our attention on the different response of second-harmonic generation to left- and right-hand circularly polarized probe beams. The circular-difference effect alone, however, does not yield the target retardation directly. The retardation can be determined only if the expansion coefficients f_i and g_i are also known. The coefficients can be calculated theoretically but the most realistic models require precise knowledge of the second-order susceptibility tensor and of the refractive indices of the materials. To avoid these theoretical problems, we determined the expansion coefficients experimentally for the very geometry used in the actual retardation measurements. This, in principle, allows calculation of the target retardation from the measured circular-difference effect.

In our experiments, however, we used an alternative approach in which a quarter-wave plate is rotated continuously to access a range of probe polarization states including the circular ones. The recorded polarization line shape is then fitted by use of a prescribed model and the measured values of f_i and g_i, yielding the retardation of the target wave plate directly. This approach is superior to that based on the circular-difference response alone, because the polarization line shape is sensitive to the details of the experiment and contains information that allows verification of the proper operation of the setup.

We consider a situation in which the fundamental beams before the wave plates are p polarized. The polarization components of the target beam after the wave plate (arbitrary retardation δ, oriented at 45°) are given by Eqs. (22). Equations (20) and (21) with $\delta = \pi/2$ yield the components of the probe beam after the quarter-wave plate:

$$E_{2p} = [1 - i\cos(2\phi)]E_{2p}^0,$$
$$E_{2s} = -i\sin(2\phi)E_{2p}^0, \tag{30}$$

where E_{2p}^0 is the probe amplitude before the wave plate. Rotation angles of $\phi = \pm 45°$ correspond to circular probe polarizations. By inserting Eqs. (30) into Eqs. (7) and (8), we obtained a model for the second-harmonic intensity as a function of the rotation angle of the probe wave plate:

$$I \sim [f_p^2\cos^2(\delta/2) + g_s^2\sin^2(\delta/2)](1 + \cos^2 2\phi) + [f_s^2\cos^2(\delta/2) + g_p^2\sin^2(\delta/2)]\sin^2 2\phi + (f_s g_s - f_p g_p)\sin\delta\sin 2\phi. \tag{31}$$

As explained before, we verified experimentally the absence of phase differences between coefficients f_i and g_i. Since our method is insensitive to absolute phase, we consider all expansion coefficients to be real. Formula (31) is then used to fit the recorded polarization line shape and allows a precise determination of target retardation δ. Note that retardation is the only fit parameter in the model of formula (31), except for a mere scaling factor for the absolute signal level.

To address possible phase differences between the expansion coefficients further, we developed a more general model that allows for complex expansion coefficients in

Eqs. (7) and (8). For a fixed target polarization, intensity I of the second-harmonic signal is then of the form

$$I \sim a|E_{2p}|^2 + b|E_{2s}|^2 + (c + id)E_{2p}E_{2s}^* + (c - id)E_{2p}^*E_{2s}. \quad (32)$$

The real coefficients a, b, c, and d include both the polarization components of the target field and the complex coefficients f_i and g_i. Using Eqs. (30) we obtained the signal intensity as a function of rotation angle ϕ:

$$I \sim a[1 + \cos^2(2\phi)] + b\sin^2(2\phi) + c\sin(4\phi) - 2d\sin(2\phi). \quad (33)$$

As a matter of fact, formula (32) is valid for an arbitrary sample symmetry. Hence, formula (33) determines the fit quality of any recorded polarization line shape. A nonvanishing value of c in formula (33) indicates phase differences between coefficients f_i and g_i.

7. EXPERIMENTAL DETAILS

In our experiments we used a spin-coated thin film (~250 nm thick) of the side-chain polyimide A-095.11 (Sandoz). After spin coating, the nonlinear chromophores are randomly oriented. The sample was poled to produce a net alignment of the chromophores and to obtain a second-order response, while preserving the in-plane isotropy of the film ($C_{\infty v}$ symmetry). The principal absorption maximum of the polymer was at 502 nm and its refractive index at the fundamental wavelength (1064 nm in our experiments) was approximately 1.676.

The experimental setup for retardation measurements is shown in Fig. 4. Infrared light from a Q-switched Nd:YAG laser (1064 nm, ~5 mJ, 10 ns, 30 Hz) was split into two beams of nearly the same intensity (target and probe). Calcite Glan polarizers (~4×10^{-6} extinction ratio) were used to polarize each beam separately along the p direction. The polarization of the probe beam was varied by means of a quarter-wave plate and the nominal half-wave plate to be tested was placed in the target beam. Zero-order wave plates were used because of their

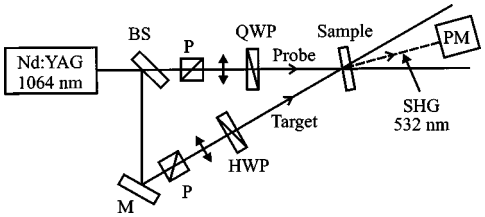

Fig. 4. Experimental setup for retardation measurements. Laser light at 1064 nm is split into two beams (target and probe). After the beam splitter (BS), the beams are p polarized by Glan polarizers (P). The polarization of the probe beam is varied by a zero-order quarter-wave plate (QWP). The nominal half-wave plate (HWP) to be investigated is placed in the target beam. The beams are applied to the same spot of a poled polymer film and second-harmonic light at 532 nm is detected by a photomultiplier (PM) in the sum direction.

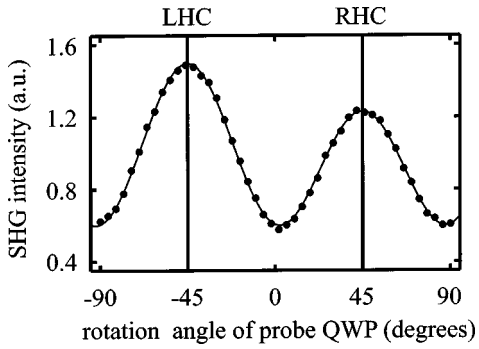

Fig. 5. Second-harmonic generation (SHG) intensity recorded continuously as the probe quarter-wave plate (QWP) is rotated. Left- (LHC) and right-hand (RHC) circularly polarized probe beams correspond to rotation angles of −45° and +45°, respectively. For this measurement, the target retardation was determined as 178.45 ± 0.03°.

better thermal stability compared with multiorder wave plates.[31] The beams were then applied to the same spot of the sample. Because of refraction at the air–polymer interface, the optimum internal incident angles were obtained with external angles of 43° and −7.5° for the target and the probe, respectively. We recorded second-harmonic light at 532 nm in the sum direction by means of a photomultiplier tube while we kept the target polarization fixed and continuously rotated the probe quarter-wave plate. The use of an analyzing polarizer was avoided to keep the setup as simple as possible.

As explained in the above sections, our technique assumes that there are no phase differences between expansion coefficients f_i and g_i. In addition, the coefficients must be known precisely. Several preliminary measurements were performed to verify that the experimental setup is properly aligned and has sufficient polarization purity to fulfill these requirements. The absence of phase differences was confirmed by the measurement of no circular-difference response when the target beam had an arbitrary linear polarization (cleaned by a Glan polarizer). The expansion coefficients were then determined for the very experimental geometry used in the subsequent retardation measurements. All the results showed that no phase differences occurred between the expansion coefficients and were in agreement with the $C_{\infty v}$ sample symmetry.

In the actual retardation measurements, the fast axis of the nominal half-wave plate to be tested was rotated by 45° from the p direction to maximize the induced ellipticity. We controlled the retardation of the target wave plate by tilting it about its fast axis.[24] We recorded polarization line shapes for a fixed target polarization by rotating the probe quarter-wave plate. The measured line shapes were first fitted with the most general model of formula (33) to address possible phase differences between the expansion coefficients further. The quality of the fits was independent of whether coefficient c in formula (33) was assumed to be zero, proving the absence of phase differences. Finally, we fitted the line shapes by using the model of formula (31) and the measured values for coefficients f_i and g_i yielding the true retardation of the target half-wave plate. A typical polarization line shape and its fit are shown in Fig. 5.

The procedure described here yielded the true retardation of the target wave plate with a precision higher than $\lambda/10^4$. Such precision results from the symmetry properties of the nonlinear interaction rather than a complicated experimental setup. The repeatability of the technique was also determined to be better than $\lambda/10^4$. These values are limited by noise in the measured line shapes and temperature fluctuations of the environment. Therefore, they can most likely be improved by refinements in the experimental details, e.g., by stabilizing the temperature of the wave plates.

8. LIMITATIONS AND APPLICATIONS

We demonstrated our technique by determining the actual retardation of a nominal half-wave plate to $\lambda/10^4$. It would clearly be interesting to measure any retardation to a similar precision. Equation (26) shows that, for a target wave plate of retardation δ oriented at 45°, the absolute circular-difference response is proportional to $\sin\delta$. Therefore, the difference depends less sensitively on retardation when this is close to $\pi/2$ or $3\pi/2$, which corresponds to circular target polarizations.

On the other hand, the sensitivity is at its maximum when the retardation is near π or 0. A retardation $\delta \cong \pi$ corresponds to the technically relevant case of a half-wave plate that we investigated in this study. Another promising application is the detection of small values of retardation ($\delta \cong 0$), for example, to measure low-level residual birefringence in optical components used in high-precision instruments.[18] An advantage of our technique is that it yields the sign of the retardation [Eq. (26)] in addition to its absolute value.

Figure 6 shows the dependence of the normalized circular-difference response [Eq. (13)] on the target retardation for the incident angles used in our experiment. Unity refractive indices for all the materials and a poling ratio of 3 for the film were assumed. When the target beam before the wave plate is p polarized, the normalization increases the sensitivity at $\delta \cong \pi$. A similar result can be achieved also at $\delta \cong 0$ if the target polarization before the wave plate is along s.

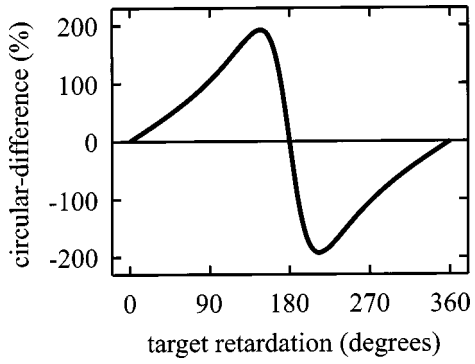

Fig. 6. Normalized circular-difference response as a function of the target retardation (simulation). The angle between the fast axis of the wave plate and the p direction was assumed to be 45°. The incident angles of the target and the probe beams were assumed to be $\theta_1 = 24°$ and $\theta_2 = -4.5°$, respectively; the refractive indices of all materials were equal and unity; and the poling ratio of the film was 3.

9. SENSITIVITY TO ERRORS

We have performed a detailed analysis of the sensitivity of our technique to various sources of error. As possible sources we considered retardation errors in the probe quarter-wave plate and misalignments of the optical components and of the fundamental beams. Assuming unity refractive indices for all the materials, a poling ratio of 3 for the film, and a fixed value for the target retardation, we simulated the second-harmonic signal allowing a deviation in one of the above parameters. The simulated line shape was fitted with the model of formula (32), which assumes an ideal experimental situation. Finally, the fitted target retardation was compared to the value assumed in the simulation. We present the results for the retardation range $\delta \sim \pi$, which corresponds to our experimental situation. Similar considerations also apply to the $\delta \sim 0$ range.

The analysis of the experimental results assumes an ideal probe quarter-wave plate. On the other hand, our technique relies on the sensitive polarization dependence of the nonlinear response. Possible retardation errors of the quarter-wave plate are therefore an important issue from the point of view of the reliability of the technique. Our error analysis shows that, for the retardation range investigated, the quality of the probe wave plate is not a limiting factor. With a deviation of $\lambda/1000$ from an ideal quarter-wave plate, e.g., the error in the determination of the target retardation is of the order of $\lambda/10^5$ for target retardations in the $180 \pm 1.2°$ range and is still less than $\lambda/10^4$ for the $180 \pm 12°$ range. Therefore, small errors in the retardation of the probe wave plate do not lead to any significant errors in the measurement of the target retardation.

We also considered the influence of the misalignment of the optical elements used to control the polarizations of the two fundamental beams. We aligned the probe and the target wave plates to within ~0.1° by placing them between two crossed calcite Glan polarizers. Our analysis shows that such misalignment of the probe quarter-wave plate does not lead to any significant error. The technique is more sensitive to the alignment of the target half-wave plate. Nevertheless, its misalignment by 0.1° results in an error of only approximately $\lambda/(5 \times 10^5)$ in the determination of its retardation. Misalignments of the linear polarizers lead to similar results. We also addressed the possibility that the beams do not lie on the same plane of incidence with respect to the sample. A misalignment of 0.06° (corresponding to a deviation of approximately 1 mm over 1 m), leads to a maximum error of $\lambda/(2 \times 10^6)$ in the retardation measurement.

The underlying reason for the inherent stability of the technique is that the circular-difference response arises from interference between the real and the imaginary parts of the fundamental field amplitudes. Clearly, the quality of the probe wave plate influences its polarization state. However, for the target retardations $\delta \sim \pi$ and $\delta \sim 0$, the (near) circular probe polarizations are princi-

pally used to detect a small imaginary component in the target polarization. Small deviations of the probe wave-plate retardation from $\delta = \pi/2$ can therefore be tolerated without a significant reduction in the precision of the technique. Nevertheless, possible retardation errors in the probe wave plate are an issue when the target retardation significantly differs from 0 or π. Misalignments of the optical components or of the beams do not introduce, to a first approximation, any additional imaginary components in the field amplitudes and do not, therefore, significantly affect the precision of the technique.

Here we have described the technique in detail for $C_{\infty v}$ sample symmetry to emphasize the salient features of the technique and because such samples are commonly available. However, the technique does not rely on this particular symmetry. If the symmetry of the sample is lower than $C_{\infty v}$, Eqs. (7) and (8) must be modified accordingly. In the most general case, eight expansion coefficients are needed to describe the second-harmonic response. However, even in this case, once phase differences between the expansion coefficients are excluded, a circular-difference effect can arise only from a phase difference between the polarization components of the target beam.

Other nonlinear polarization effects (e.g., nonlinear polarization ellipse rotation) at the fundamental or second-harmonic frequency could also influence the response.[32] However, such effects accumulate in propagation and can be neglected with a thin-film sample. For example, a typical third-order susceptibility of nonlinear polymers (10^{-10} esu) leads to a polarization azimuth rotation of 10^{-4} rad, which does not cause any appreciable error in the retardation measurements.

10. CONCLUSIONS

We have demonstrated a highly sensitive nonlinear optical technique for retardation measurements, which is based on second-harmonic generation from thin films by use of two fundamental beams. The technique relies on fundamental symmetry properties of nonlinear interactions and does not therefore require a sophisticated experimental arrangement or data analysis to achieve high precision. We presented a theoretical analysis of our technique and discussed its advantages and limitations with regard to retardation measurements. In addition, we performed a detailed analysis of the sensitivity of the technique to various sources of errors. The technique is remarkably insensitive to misalignments of the fundamental beams or of the optical components as well as to errors in the retardation of the probe quarter-wave plate. We have discussed the technique in detail for samples of $C_{\infty v}$ symmetry to emphasize its salient features while preserving mathematical simplicity. The technique can also be generalized to samples of other symmetry.

In the initial demonstration of the technique, we already achieved a precision and repeatability of better than $\lambda/10^4$ in determining the retardation of a nominal half-wave plate. We believe that these values can be further improved by future refinements in the experimental details. We are also investigating ways to extend the technique to measure arbitrary values of retardation with the same precision.

ACKNOWLEDGMENTS

This research has been supported by the Center for International Mobility and the Graduate School of Modern Optics and Photonics in Finland. We gratefully acknowledge M. Siltanen for the technical assistance, H. Tuovinen for useful discussions, as well as O. Zehnder and P. Günter for providing us with the poled polymer sample used in the experiments.

The e-mail address for M. Kauranen is martti.kauranen@tut.fi.

REFERENCES

1. S. Huard and G. Vacca, *Polarization of Light* (Wiley, New York, 1997).
2. C. Brosseau, *Fundamentals of Polarized Light: a Statistical Optics Approach* (Wiley, New York, 1998).
3. E. W. Thulstrup and J. Michl, *Elementary Polarization Spectroscopy* (Wiley, New York, 1997).
4. J. Michl, *Spectroscopy with Polarized Light* (Wiley, New York, 1995).
5. J. Tinbergen, *Astronomical Polarimetry* (Cambridge University, Cambridge, England, 1996).
6. F. T. Ulaby and C. Elachi, *Radar Polarimetry for Geoscience Applications (Remote Sensing)* (Artech House, Norwood, Mass., 1990).
7. See, for example, J. Hecht, *Understanding Fiber Optics* (Prentice-Hall, Englewood Cliffs, N.J., 1999).
8. M. Born and E. Wolf, *Principles of Optics* (Pergamon, London, 1980).
9. A. R. Bungay, S. V. Popov, and N. I. Zheludev, "Specular nonlinear anisotropic polarization effect along fourfold crystal symmetry axes," Opt. Lett. **20**, 356–358 (1995).
10. S. C. Read, M. Lai, T. Cave, S. W. Morris, D. Shelton, A. Guest, and A. D. May, "Intracavity polarimeter for measuring small optical anisotropies," J. Opt. Soc. Am. B **5**, 1832–1837 (1988).
11. F. Brandi, E. Polacco, and G. Ruoso, "Stress-optic modulator: a novel device for high sensitivity linear birefringence measurements," Meas. Sci. Technol. **12**, 1503–1508 (2001).
12. J. Y. Lee, H-W. Lee, J. W. Kim, Y. S. Yoo, and J. W. Hahn, "Measurement of ultralow supermirror birefringence by use of the polarimetric differential cavity ringdown technique," Appl. Opt. **39**, 1941–1945 (2000).
13. *Polarization Solutions, 2001–2002 Catalog* (Meadowlark Optics, Frederick, Colo., 2001).
14. L. Yao, Z. Zhiyao, and W. Runwen, "Optical heterodyne measurement of the phase retardation of a quarter-wave plate," Opt. Lett. **13**, 553–555 (1988).
15. S. Nakadate, "High precision retardation measurement using phase detection of Young's fringes," Appl. Opt. **29**, 242–246 (1990).
16. K. B. Rochford and C. M. Wang, "Accurate interferometric retardance measurements," Appl. Opt. **36**, 6473–6479 (1997).
17. Y. Zhang, S. Zhang, Y. Han, Y. Li, and X. Xu, "Method for the measurement of retardation of wave plates based on laser frequency splitting technology," Opt. Eng. **40**, 1071–1075 (2001).
18. B. Wang and T. C. Oakberg, "A new instrument for measuring both the magnitude and angle of low level linear birefringence," Rev. Sci. Instrum. **70**, 3847–3854 (1999).
19. B. Wang and W. Hellman, "Accuracy assessment of a linear birefringence measurement system using a Soleil–Babinet compensator," Rev. Sci. Instrum. **72**, 4066–4070 (2001).
20. T. Petralli-Mallow, T. M. Wong, J. D. Byers, H. I. Yee, and J. M. Hicks, "Circular dichroism spectroscopy at interfaces:

a surface second harmonic generation study," J. Phys. Chem. **97**, 1383–1388 (1993).
21. M. Kauranen, T. Verbiest, and A. Persoons, "Second-order nonlinear optical signatures of surface chirality," J. Mod. Opt. **45**, 403–423 (1998).
22. M. Kauranen, S. V. Elshocht, T. Verbiest, and A. Persoons, "Tensor analysis of the second-order nonlinear optical susceptibility of chiral anisotropic thin films," J. Chem. Phys. **112**, 1497–1502 (2000).
23. S. M. Saltiel, P. D. Yankov, and N. I. Zheludev, "Second harmonic generation as a method for polarizing and analyzing laser light," Appl. Phys. B **42**, 115–119 (1987).
24. S. Cattaneo, O. Zehnder, P. Günter, and M. Kauranen, "Nonlinear optical technique for precise retardation measurements," Phys. Rev. Lett. **88**, 243901 (2002).
25. J. D. Jackson, *Classical Electrodynamics* (Wiley, New York, 1975).
26. Y. R. Shen, *Principles of Nonlinear Optics* (Wiley, New York, 1984).
27. T. Verbiest, M. Kauranen, and André Persoons, "Light-polarization-induced optical activity," Phys. Rev. Lett. **82**, 3601–3604 (1999).
28. J. E. Sipe, "New Green-function formalism for surface optics," J. Opt. Soc. Am. B **4**, 481–489 (1987).
29. Ch. Bosshard, K. Sutter, Ph. Prêtre, J. Hulliger, M. Flörsheimer, P. Kaatz, and P. Günter, *Organic Nonlinear Optical Materials* (Gordon & Breach, Basel, Switzerland, 1995).
30. R. M. A. Azzam and N. M. Bashara, *Ellipsometry and Polarized Light* (North-Holland, Amsterdam, 1989), p. 488.
31. P. D. Hale and G. W. Day, "Stability of birefringent linear retarders (waveplates)," Appl. Opt. **27**, 5146–5153 (1988).
32. Yu. P. Svirko and N. I. Zheludev, *Polarization of Light in Nonlinear Optics* (Wiley, New York, 1998).